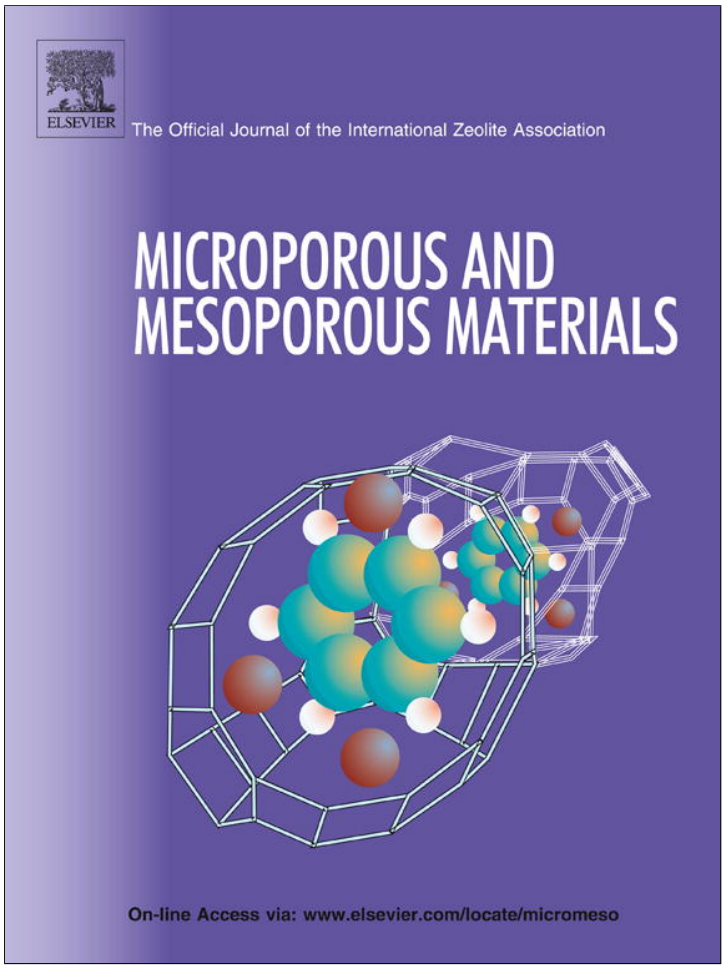

Microporous and Mesoporous Materials 177 (2013) 113–119

Contents lists available at SciVerse ScienceDirect

Microporous and Mesoporous Materials

journal homepage: www.elsevier.com/locate/micromeso

Cation site preference in zeolite clinoptilolite: A density functional study

Ellie L. Uzunova [a,*], Hans Mikosch [b]

[a] Institute of General and Inorganic Chemistry, Bulgarian Academy of Sciences, Sofia 1113, Bulgaria
[b] Institute for Chemical Technologies and Analytics, Vienna University of Technology, Getreidemarkt 9/E164-EC, A-1060 Vienna, Austria

ARTICLE INFO

Article history:
Received 9 January 2013
Received in revised form 19 April 2013
Accepted 4 May 2013
Available online 13 May 2013

Keywords:
Clinoptilolite
Cations migration
ONIOM
Periodic structure
DFT functional calculations

ABSTRACT

The structure of zeolite clinoptilolite and the coordination of extraframework cations (Ca^{2+}, Ba^{2+}, Na^{+} and K^{+}) by framework oxygen atoms are examined by density functional theory (DFT) using two methods: the ONIOM two-layer model (DFT/MM) and periodic DFT. Both ONIOM and periodic model calculations predict correctly the clinoptilolite structure and find configurations with Al → Si substitution at the T2 site which interconnects the *xz* layers via its apical oxygen atom as the most stable ones, in agreement with experimental data. The configurations with Al → Si substitution at the T1 sites are favorable for migration of cations into the large channel A from the eight-member rings which are side rings of channel A and opened in channel C (c-rings); the process is energetically most favorable for the Na^{+} cations. K^{+} and Ba^{2+} cations occupy sites in the vicinity of the c-rings: M1, M1a and M3, among which K^{+} prefers the M3 site inside the c-rings. The molecular electrostatic potential (MEP) maps reveal areas of increased nucleophilic properties inside the large channel A, to which cations can migrate upon heating, or incoming cations can be retained. The minimal interatomic distances between two equivalent cations, residing in channel A are 4.850 Å (Ca^{2+}–Ca^{2+}); 5.025 Å (Na^{+}–Na^{+}) and 4.305 Å (K^{+}–K^{+}). The ONIOM method should be preferred over periodic models for describing cations in the c-rings: the smaller c-parameter of the unit cell replicates the cations in adjacent rings along the [001] direction.

1. Introduction

Clinoptilolite is the best known natural zeolite, explored in numerous industrial applications as adsorbent, ion-exchanger and supporting material, as it can be found in large deposits worldwide [1]. The extraframework cations in zeolites, which compensate the negative framework charge, resulting from Al → Si substitutions, do not always have fixed crystallographic positions; they are located in the zeolite pores and are easily exchangeable, thus providing the valuable application of zeolites as ion-exchangers. Clinoptilolite is isomorphous with heulandite and the framework bears the HEU three-letter zeolite notation [2]. Heulandite and clinoptilolite are distinguished based on the Si/Al ratio, clinoptilolite being the Si-rich structure with Si/Al > 4. The clinoptilolite unit cell consists of 108 framework atoms and commonly 4–7 extraframework cations M^{n+}, which balance the negatively charged framework, $(M^{n+})_{x/n}Si_{36-x}Al_xO_{72}$. Extensive experimental studies have been performed on the structure stability, Si, Al ordering and extraframework cation locations [3–13]. The cation mobility of Na^{+}, K^{+} and Cs^{+} cations in clinoptilolite was studied by *in situ* X-ray diffraction and molecular dynamics [13]. Zeolite basicity is related to the presence of alkali and alkaline-earth cations, which form bonds with the framework oxygen atoms bearing pronounced ionic character [14]. The extraframework cations act as electrophiles, while the framework oxygen atoms retain their nucleophilic character. Alkali cation exchanged FAU zeolite presented activity in the reaction of N_2O_4 disproportionation, which was examined by density-functional methods with cluster models and by applying periodic boundary conditions (PBC) [15]. The nature of the active centers in the faujasite supercage and the role of cooperative action from extraframework cations and confinement of the reactant by the zeolite framework were revealed. The necessity to have alkali cations at sites SIII in FAU was emphasized [15,16]. Natural zeolites, however, are used as adsorbents rather than catalysts and for clinoptilolite theoretical studies from first principles have not been applied so far. Earlier theoretical representations of clinoptilolite and heulandite were based on atomistic simulations using empirical static lattice models; they examined the Si, Al ordering in relation to the cation distribution, thus revealing the relative stability of different cation coordination [17,18]. While such models are excellent to predict structural properties, chemical reactivity and physical properties such as dielectric constants are far more accurately determined by electronic structure methods. The relatively large unit cell of clinoptilolite and the fact that extraframework cations are not confined in small rings, for which cluster methods could be used, are the main reasons why *ab initio* calculations have not been performed yet.

* Corresponding author. Tel.: +359 29793793; fax: +359 28705024.
E-mail address: ellie@svr.igic.bas.bg (E.L. Uzunova).

1387-1811/$ - see front matter © 2013 Elsevier Inc. All rights reserved.
http://dx.doi.org/10.1016/j.micromeso.2013.05.003

The advantages of *ab initio* methods for studying the structure and reactivity of zeolites and density functional theory (DFT) in particular, have been outlined and many zeolite structures have been successfully described by using either finite or periodic models [15,16,19–26]. The tetrahedral atoms of the zeolite framework form covalent bonds with oxygen atoms, but the framework bears a negative charge and forms ion-pairs with the extraframework cations. The negative charge is certainly not localized at the T centers where the Al → Si substitutions occur; it is delocalized over the bridging oxygen atoms. The degree of delocalization of the framework charge strongly depends on the type of building units [19,23–25]. The DFT studies provide unique insight into the local environment of an extraframework cation or active center, the electron density and charge distribution and how the Si, Al ordering affects the bonding of different cations to the negatively charged lattice [19]. Zeolites and microporous materials which have unit cells of 20–40 atoms, like sodalite, zeolite A, ALPO-34 (CHA topology), allow full structure optimization using DFT methods [19,20,26]. Zeolite clinoptilolite has a larger unit cell and a major application is the retention of heavy metal cations and nuclear wastes removal, which would render periodic computational studies as highly expensive. It has been shown, however, that the embedded cluster model using ONIOM allow accurate calculations at lower computational costs [23,27–29]. The common cations, found in natural clinoptilolite and heulandite, are Na^+, K^+, Ca^{2+}; [3–9] Ba^{2+} containing natural heulandite was also reported [11]. In the present study, we present the results of both methods: a two-layer ONIOM model and periodic boundary conditions (PBC) in the optimization of clinoptilolite with Na^+, K^+, Ca^{2+} and Ba^{2+} as extraframework cations. The relative stability of Si, Al orderings and the cation distributions arising from specific Si, Al substitutions are examined; the binding of cations to lattice oxygen is compared as revealed by ONIOM and PBC. The cation mobility, which has been a subject of experimental studies, is also assessed.

2. Structure and methods

The structure of clinoptilolite is monoclinic (space group C2/m) and consists of four- and five-member rings; eight- and ten-member rings define the channel system. A larger SBU is identified, denoted as 4–4 = 1 and shown in Fig. 1. Five non-equivalent tetrahedral positions are distinguished. The T5 tetrahedron interconnects the SBUs to form a chain parallel to the *z*-axis and the chains are linked by oxygen atoms bonded to four-member rings so as to form sheets. In both clinoptilolite and heulandite these sheets (periodic building units) are related by rotation of 180° about the *y*-axis and linked by T2–O1–T2 bridges. A 2D pore system is formed in the [0 1 0] plane, with three main channels: A (10-member ring), B (symmetric 8-member ring) and C (8-member-ring), of which A and B run in direction to the c-axis, while channel C intersects both channels A and B

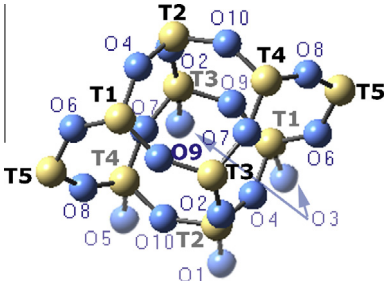

Fig. 1. The 4–4 = 1 SBU in clinoptilolite with T and O atom numbering according to Refs. [4,10,11]. Oxygen atoms are blue, Si – light brown. (For interpretation of the references to color in this figure legend, the reader is referred to the web version of this article.)

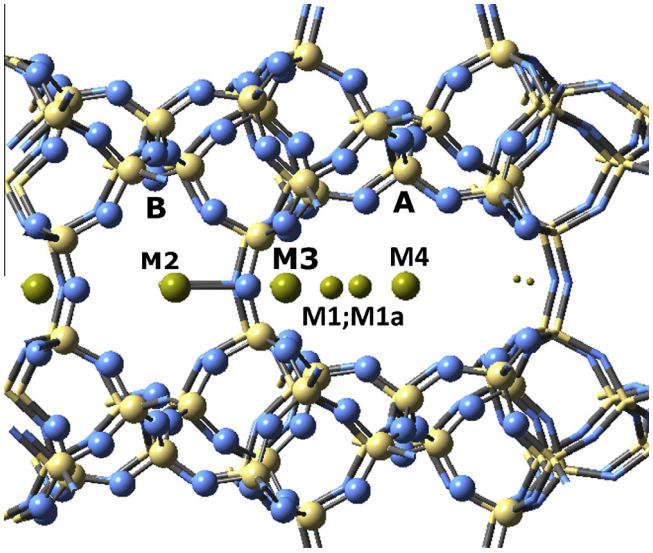

Fig. 2. The clinoptilolite structure viewed along the c-vector with the main channels A and B and the extraframework cation sites. Oxygen atoms are blue, Si – light brown, extraframework cations are light green. (For interpretation of the references to color in this figure legend, the reader is referred to the web version of this article.)

and is parallel to the a-axis. Three main cation sites are occupied by alkali and alkaline-earth cations, two of them located in channel A, coordinated to oxygen atoms from the side 8-member ring, M1 and M3, and one in channel B, M2, Fig. 2. A fourth site M4 with much lower occupancy was distinguished for small-sized hydrated cations in the center of channel A. The difference between sites M1 and M3 is that M3 are more confined within the side eight-member ring and less exposed to the channel. The sites M1 and M1a are shifted in direction to the channel center and M1a is weakly coordinated by atoms from the side-ring, but closer to the T1–O4–T2 and T1–O6–T5 linkages of the 10-member ring in channel A, Fig. 3.

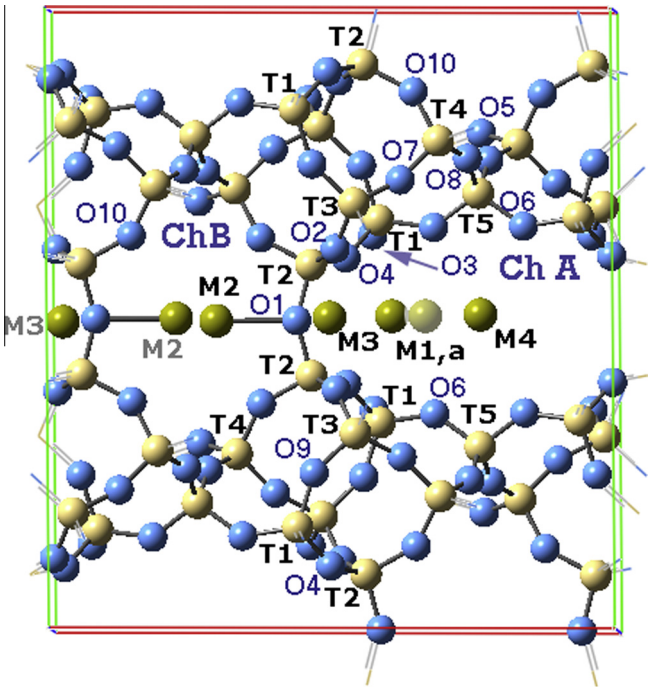

Fig. 3. The clinoptilolite unit cell with cation sites and framework atom numbering (see also Fig. 1). Oxygen atoms are blue, Si – light brown, extraframework cations are light green. (For interpretation of the references to color in this figure legend, the reader is referred to the web version of this article.)

The charge arising from single Al → Si substitutions was compensated by monovalent cations and double substitutions at different T-sites were balanced by the Ca^{2+} cations. The T2–T2′ internuclear distance in the side 8-member rings, as well as the O1–O1′ distance correspond to the length of the c-vector and this should be taken into account when studying Si, Al orderings with T2 substitutions by applying periodic models. Any substitution at a T2 site is replicated at the opposite side of the ring, (Fig. 4a).

The periodic calculations were performed with Gaussian 09 using the PBE density functional [30–32]; the Brillouin-zone sampling was restricted to the Γ point. All electrons were explicitly included in the periodic DFT calculations. In studies of polysiloxanes, the importance of applying polarization functions for T-atoms (Si, Al), rather than for oxygen, has been stressed [21], therefore we have used the standard 3–21G* basis set with added polarization functions for the second row elements (Si, Al); the extraframework cations were described by the 6–31G(d) basis set [33–37]. The charge distributions were examined by natural bond orbital (NBO) analysis, which yields results that are rather insensitive to basis set enlargement and reveals both covalent and non-covalent effects in molecules [38,39].

A two-layer model was adopted for the ONIOM calculations, QM/MM [27–29,40,41]. Geometry optimizations were performed using the "quadratic macro coupling" method, which couples forces between the QM and MM layers in a numerically stable way [29,40]. For the high-layer the B3LYP hybrid density functional and the 6–31G(d) basis set were applied for all atoms except the Ba^{2+} cations for which the split-valence QZVP basis and the corresponding pseudopotential for the core electrons were applied [42,43]. Hybrid functionals, such as B3LYP [44–46], can better describe the properties of zeolites and aluminosilicates, which are large band-gap insulator materials, but they are prohibitively expensive for PBC calculations. The universal force-field was applied for describing the low layer and the terminal atoms were fixed at crystallographic positions [28,47]. Si/Al ratios in the range 4.5–9.0 were examined and ONIOM models of different size were tested: the largest one consisted of 16T/100T atoms and it was used to derive the electrostatic potential in the zeolite channels and the relative stability of configurations, Fig. 5. 8T/76T models proved sufficient to describe cation sites M1, M2 and M3; the minimal model for describing cation migration in the large channel is 10T/100T. Throughout the tables, results from 16T/100T models are presented. Frequency calculations were performed for the finite models in order to justify the optimized configurations as points of energy minima. The electrostatic potential (ESP) of the clusters was calculated from the B3LYP density and molecular electrostatic potential (MEP) maps were derived in which areas of enhanced reactivity in the zeolite structure can be discerned.

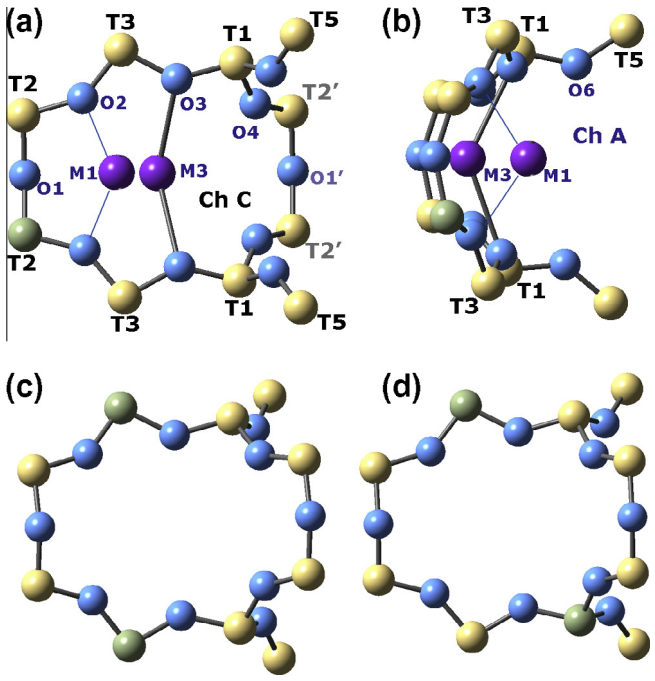

Fig. 4. The side eight-member ring with the cation sites M1 and M3 exposed in channel A. (a) viewed along [100], (b) viewed along [001]. (c) Ca^{2+} at site M1 and Al → Si substitutions at T3 sites predicted as the most stable configuration by ONIOM. (d) Ca^{2+} at site M1 and Al → Si substitutions at T1-T3 sites, predicted as the most stable configuration by PBC. Oxygen atoms are blue, Si – light brown, Al – green, extraframework cation positions are dark blue, Ca^{2+} cations are light green. (For interpretation of the references to color in this figure legend, the reader is referred to the web version of this article.)

3. Extraframework cation locations related to the Si, Al ordering at tetrahedral sites in clinoptilolite

3.1. Framework properties, determined by ONIOM and PBC calculations

The symmetry of the clinoptilolite framework is lowered from C/2m to Cm or even C1, when Al → Si substitutions are considered. The flexibility of the angles TOT is very pronounced in this framework and the X-ray diffraction (XRD) studies reported a range of

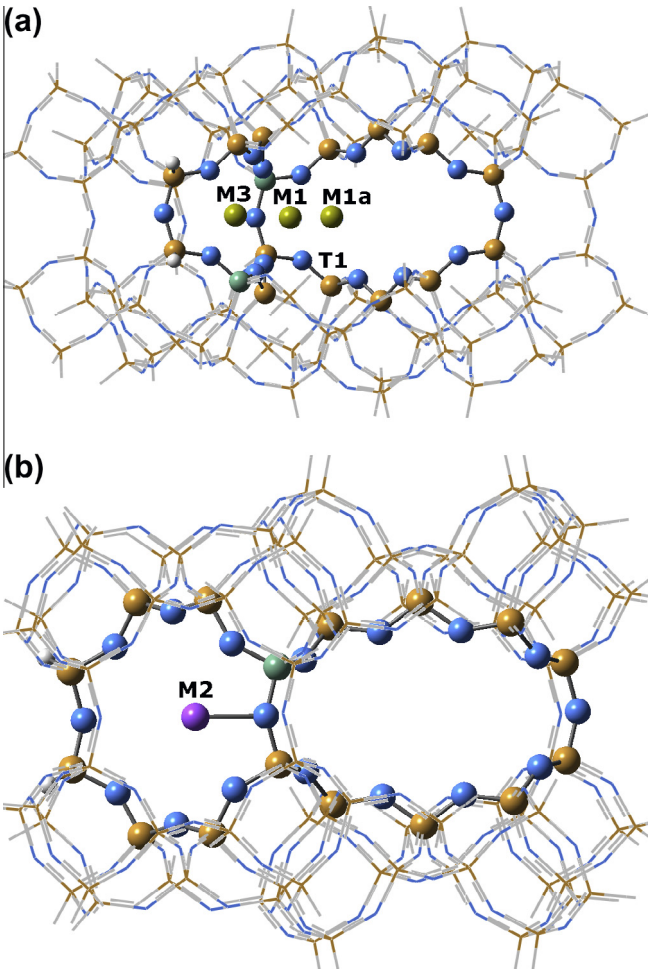

Fig. 5. The 16T/100T ONIOM models with the main cation sites. The low layer, described by molecular mechanics (MM) is shown as wireframe. (a) Sites in channel A, (b) Sites in channel B.

Table 1
Bond lengths (Å) and bond angles (TOT, deg) in proximity to cation sites in clinoptilolite, calculated by using ONIOM and PBC; unit cell Parameters.

Method	ONIOM			PBC		
Cation, Site	Ca(M1)	Na(M1)	K(M3)	Ca(M1)	Na(M1)	K(M3)
Si(T2)–O	1.655	1.638	1.656	1.672	1.675	1.621
Al(T2)–O	1.799	1.751	1.745	1.769	1.763	1.757
Si(T3)–O	1.646	1.657	1.663	1.663	1.653	1.673
Al(T3)–O	1.754	1.787	1.772	1.789	1.772	1.769
Si(T1)–O	1.633	1.643	1.680	1.669	1.656	1.667
Al(T1)–O	1.786	1.799	1.799	1.791	1.773	1.771
T2–O–T2	156.1	135.6	133.6	148.1	147.2	152.1
T2–O–T3	150.6	140.1	141.7	145.2	140.5	147.3
T2–O–T1	160.8	144.2	122.3	161.9	135.2	128.2
Unit cell	a = 17.612 Å, b = 17.837 Å, c = 7.416 Å, α = 88.1°, β = 113.5°, γ = 90.5° (Ca^{2+}). a = 17.674 Å, b = 17.961 Å, c = 7.417 Å, α = 87.9°, β = 113.9°, γ = 89.7° (Na^{+}). a = 17.783 Å, b = 18.153 Å, c = 7.426 Å, α = 89.7°, β = 114.3°, γ = 90.0° (K^{+}).					
Exp[a]	a = 17.660 Å, b = 17.963 Å, c = 7.400 Å, α = 90°, β = 116.47°, γ = 90.0° (Ca^{2+}). a = 17.4030(10) Å, b = 18.0120(10) Å, c = 7.4350(10) Å, α = 90.0°, β = 113.812(2)°, γ = 90.0° (Na^{+}). a = 17.688(16) Å, b = 17. 902(9) Å, c = 7. 409(7) Å, α = 90°, β = 116.50(7)°, γ = 90.0° (K^{+}).					

[a] Experimental unit cell parameters are from Refs. [4,13,56].

136–160° [4,10]. Based on the experimentally determined elongation of the T2–O bonds by XRD and neutron diffraction [4,48,49], high level of Al → Si substitutions at the T2 site (40%) was suggested and atomistic simulations confirmed the higher stability of such configurations [17]. In a pure siliceous framework, our PBC calculations indicate some elongation of the T2–O bonds within the c-rings: 1.649 Å for T2–O4 and 1.639 Å for T2–O2 vs an average Si–O distance of 1.631 Å. Both the ONIOM and PBC calculations predict an elongation of the T–O bonds upon Al → Si substitution within the range 0.10–0.15 Å, the largest deviations being observed at T1 sites, Table 1. The monovalent cations Na^{+} and K^{+} have preference to different sites in the large channel A, M1(Na^{+}) and M3(K^{+}), respectively, the latter site being more confined within the c-ring, Fig. 4. The angles TOT in proximity to cation sites undergo strong deformation. Na^{+} and Ca^{2+} cations have similar crystal and ionic radii, while the K^{+} cation is considerably larger [50]. Thus, K^{+} cations can reach optimal coordination within the side eight-member rings and they were found to occupy predominantly the M3 sites in hydrated clinoptilolite, while Na^{+} cations would prefer the M1 site [4]. According to our calculations, the presence of K^{+} cations at M3 sites leads to sharpening of the angles T2–O–T1, while Na^{+} cations at M1 sites cause moderate deformation of both the T2–O–T1 and T2–O–T3 angles. An increase of the unit cell parameters is observed for K-exchanged clinoptilolite, most significant in the [010] direction. The ONIOM and PBC results differ regarding the T2–O–T2 angle deformation in presence of Na^{+} and K^{+} cations, the ONIOM results indicating stronger ring deformation than PBC. Both methods agree that while the monovalent cations lead to sharpening of the T2–O–T1 angle, Ca^{2+} cations contribute to its significant widening. The Na^{+} cations show less-pronounced preference towards different Si, Al orderings and they approach the framework negative charge, forming shorter M-O bonds as compared to the other cations. The T2 position is in proximity to the M1, M2 and M3 cation sites, Fig. 2, and Al positioned at T2 is the favored Al location for Na^{+} cations at either the M1 or M2 sites, Table 2. For K^{+} cations ONIOM and PBC predict different optimal Al site occupancy: T1 is favored by ONIOM, while T1 and T2 are nearly isoenergetic at the PBC level. The energy difference between the configurations involving K^{+} cations is larger for the ONIOM models, while the T1, T2 and T3 site occupancies by Al, when compensated by K^{+} at site M3, appear with similar energies according to the PBC results. The periodic models for M3 site occupancy do not describe accurately the framework, because they imply replications of both Al → Si substitution and cation site position in adjacent c-rings, moreover, any T2 substitution is replicated at the T2′ position of the same ring, Fig. 4. The c-rings of the PBC optimized lattice undergo deformation of T2–O–T2′ angles, when the M3 site is occupied by a cation and the replicated cations in the adjacent cells appear at close distances along the [001] direction, which equal in length the c-parameter. The c-parameter of the clinoptilolite unit cell is more than twice smaller compared to the a- and b-parameters and it is typically in the range 7.40–7.45 Å, and the cations would appear as regularly ordered and closely spaced along channel C, Fig. 6. The same effect should be expected for zeolite mordenite, whose unit cell is also narrow in one direction and the ratios a/c and b/c are even higher than in clinoptilolite [2]. The ONIOM model represents in a more realistic way K-exchanged clinoptilolite, as it avoids cation crowding in the C-channel rings. The ONIOM and PBC results agree however, for a second possible cation location denoted as M1a, which is considerably shifted towards the center of channel A and becomes energetically favorable upon Al → Si substitutions at the T1 site, Figs. 4b and 5a.

As the most stable framework configuration to host divalent Ca^{2+} cations, both ONIOM and PBC predict the M1 site with location of the negative framework charges at the opposite long sides of the asymmetric side eight-member ring, but while ONIOM predicts a T3–T3 occupancy for Al as the one of lowest energy, PBC predicts T1–T3, Fig. 4b and c. This discrepancy can be again explained by the narrow size of the cell along [001] and the consideration of double Al → Si substitutions in neighboring c-rings. The Si, Al orderings with Al substitution at a T2 site have lower stabilization energy estimated by PBC, than by ONIOM, except for Al → Si substitutions at T2, T4 sites, as the T4 site does not belong to the c-rings. According to the ONIOM calculations, Al → Si substitutions [T2(Al)–O–$(SiO)_2$–T2′(Al)] within the c-ring are energetically unfavorable, moreover, in a highly siliceous framework this is unlikely to occur, Table 2S, (Supplementary material). The M2 site occupancy by Ca^{2+} is also predicted to be energetically more favorable by ONIOM than by PBC, the latter separating it from all other configurations by a large energy gap, Table 2. XRD studies of Al-rich heulandite found Ca^{2+} predominantly at M1 and M3 sites, while in the Si-rich clinoptilolite, most of the Ca^{2+} cations occupied the M2 sites [4,10]. The calculated natural charges indicate more significant polarization for the smaller cations (Ca^{2+} and Na^{+}), while K^{+} forms predominantly ionic bonds, Table 3. This can be explained by the ability of the small-sized cations to approach the centers of negative framework charge and in this way to reach optimal coordination by the nearest framework oxygen atoms. The Na^{+} cations form bonds with more pronounced ionic character, when residing at the M2 site, while at all other cation sites, their interactions with the lattice are stronger. In the proximity to a negative framework charge, the partial charges at tetrahedral atoms are higher, indicating the locally increased ionic character of the bonds within the framework. The Al → Si substitution at T5 sites is the least favorable for

Table 2
Cation-lattice oxygen internuclear distances R_{MO} (Å) for different cation sites and the most favorable nearest Si, Al orderings.[a] Relative stability estimated by total energy difference.

Configurations/linkages[b]	ONIOM		PBC	
Ca(II) at M1	R_{MO}	ΔE_{tot}, kJ mol^{-1}	R_{MO}	ΔE_{tot}, kJ mol^{-1}
Al at T1, T3 -AlO(SiO)$_3$Al–	2.353, 2.387, 2.411, 2.666	25.2	2.338, 2.377, 2.385, 2.388	0.0
2Al at T3–AlO(SiO)$_2$Al–	2.342, 2 × 2.398	0.0	2.392, 2 ×2.398	40.0
Al at T2, T3–AlOSiOAl–	2.334, 2.358, 2.612, 2.673	39.6	2.377, 2.409, 2.524, 2.664	24.4
2Al at T1–AlO(SiO)$_2$Al– Ca(II) at M1a	2 × 2.361, 2 × 2.427	44.4		
2Al at T1–AlO(SiO)$_2$Al– Ca(II) at M2	2.309, 2.328, 2.357, 2.400	55.3	2 × 2.354 2 × 2.460	50.9
Al at T2, T4–AlOSiOAl– Ba(II) at M1	2.305, 2.338, 2.374	69.9	2.391, 2.414, 2.431, 2.435	97.7
2Al at T3–AlO(SiO)$_2$Al– Ba(II) at M1a	2.562, 2.563, 2.995, 2.998	0.0		
2Al at T1–AlO(SiO)$_2$Al– Ba(II) at M2	2.556, 2.531, 2.849, 2.944	32.2		
Al at T2, T4–AlOSiOAl– Na(I) at M1	2.504, 2.591, 2.710	55.1		
Al at T2	2.210, 2.417	0.0	2.290, 2.409, 2.687	0.0
Al at T1	2.237, 2.307	8.9	2.266, 2.277, 2.360, 2.454	3.2
Al at T3	2.291, 2.444	29.0	2.254, 2.415, 2.645	27.6
Na(I) at M1a; Al at T1	2.143, 2.325	11.0	2.199, 2.428, 2.511	7.6
Na(I) at M1a; Al at T2	2.193, 2.315, 2.476	18.5		
Na(I) at M2; Al at T2	2.206, 2.240	49.2	2.185, 2.331, 2.341	66.8
K(I) at M3				
Al at T1	2.691, 2.707	0.0	2.785, 2.855, 2.992	2.0
Al at T2	2.712, 2.971	50.2	2.850, 3.022	0.0
Al at T3	2.656	33.4	2.780, 2.795	13.7
K(I) at M1a Al at T1	2.765, 2.745	66.3	2.641, 2.772, 2.847	27.7
K(I) at M2; Al at T2	2.583, 2.604	129.0	2.697, 2.856, 2.889	56.8

[a] A full list with all Si, Al orderings stabilizing the different cations, as well as ONIOM calculations using PBE are presented as Table S1 in Supporting information.
[b] Al → Si substitutions separated by Si-occupied T-sites. The lowest energy configurations are taken as reference zero.

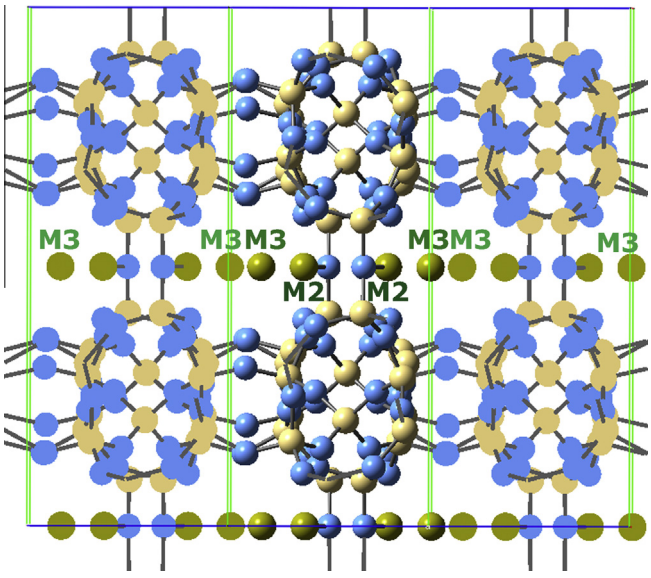

Fig. 6. The clinoptilolite structure viewed along [0 0 1] with the C channel and the extraframework cation sites. Oxygen atoms are blue, Si – light brown, extraframework cations are light green. The replicated cell is shown as wireframe. (For interpretation of the references to color in this figure legend, the reader is referred to the web version of this article.)

stabilizing both small-size and large-size cations (Table 2S, Supporting information) and this agrees with the experimental findings [4,10,14]. The cations do not find proper coordination at the center of the Channel A (sites M4), but they are shifted towards the T5 site.

Table 3
Natural charges on tetrahedral atoms and extraframework cations for PBC optimized structures.

Atom	Charge
Si	1.84 ÷ 2.12
Al	1.45 ÷ 1.56
O (Al–O)	−1.11 ÷ −1.17
O (Si–O)	−1.05 ÷ −1.07
Na^+ at M2	0.78
Na^+ at M1, Al at T2	0.71
Na^+ at M1, Al at T1	0.65
Na^+ at M1a	0.74
K^+ at M2	0.82
K^+ at M3, Al at T2	0.80
K^+ at M3, Al at T1	0.80
K^+ at M1a	0.77
Ca^{2+} at M2	1.37
Ca^{2+} at M1	1.37

The ONIOM calculations with Ba^{2+} as extraframework cation indicate two main positions: M1 and M2, of which the M1 site is preferred. Ba^{2+} forms lengthened bonds to framework oxygen atoms, thus the M1 site with Ba^{2+} is located more closely to the inner space of channel A, compared to Ca^{2+}. Al → Si substitution at T1 site would result in shifting of the Ba^{2+} cation to the M1a site; the energy required is 32 kJ mol^{-1} thus Ba^{2+} would more easily become exposed inside channel A, than K^+, but Ba^{2+} migration is less likely to occur compared to Ca^{2+} or Na^+, Table 2. The preference of Ba^{2+} cations to occupy M1 sites was also experimentally observed, and a similar trend was found for Sr^{2+} cations [11,12].

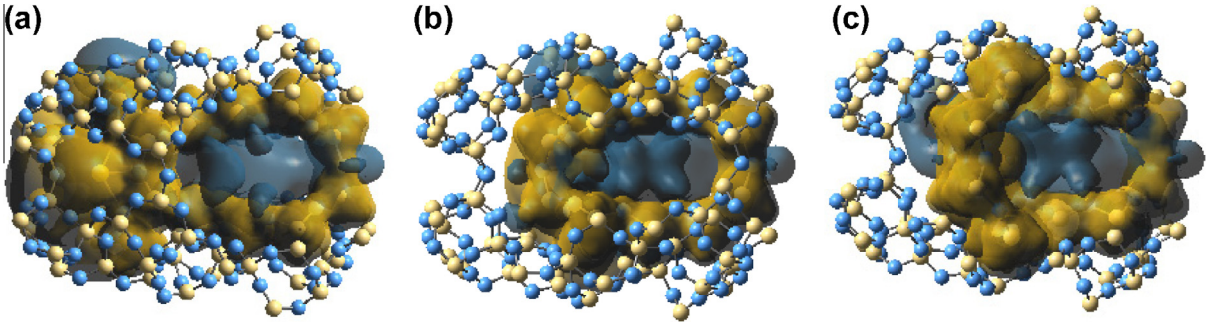

Fig. 7. The MEP maps with different cations positioned at the highly populated cation sites. (a) Ca^{2+} at site M2, (b) Ca^{2+} at site M1, (c) K^+ at site M3. Areas of positive EP (electrophilic) are yellow, the negative EP (nucleophilic) are displayed in blue. (For interpretation of the references to color in this figure legend, the reader is referred to the web version of this article.)

3.2. Electrostatic potential inside the channels of clinoptilolite. Cation migration

In charged frameworks, such as zeolites, it is important to derive the electrostatic potential within the cavities, because all adsorption, diffusion and catalytic processes pass through the channels. ESP is a better indicator for zeolite reactivity than charge distribution or bond population as it is much less dependent on the choice of basis set [51,52]. The molecular electrostatic potential (MEP) maps calculated in the presence of cations at M1, M2 and M3 sites clearly indicate regions of enhanced nucleophilicity inside channel A, to where cations can migrate from their original positions, or incoming cations can be retained, Fig. 7. Areas of positive ESP are concentrated in the vicinity of the cations. Despite the concentration of cations inside channel C, permeability for cations is retained, evidenced by narrow continuous areas of negative ESP. A broader area of negative ESP is developed in the presence of K^+ cations, which penetrates also part of channel B. Though the exchange capacity of clinoptilolite towards a number of cations was subject of experimental studies [5,53–55], the zeolite reactivity and potential inside the channels were not assessed by theoretical methods so far. Clinoptilolite is more stable under thermal treatment than the Al-rich framework of heulandite. Nevertheless, cation migration was observed in Na^+ and Cs^+ exchanged clinoptilolites [13]. The Na^+ cations tend to leave the c-rings at elevated temperature (300 °C) and occupy the inner space of channel A, including site M4 in the center of the 10-member ring.

Numerous studies were devoted to K-exchanged heulandites, as it was found that the presence of K^+ cations improves the stability of heulandite [4,9,56]. A similar tendency of K-cations to migrate towards the center of channel A was observed upon dehydration of heulandites and before structure collapse [9]. The positions of K^+ and Na^+ cations after their migration inside channel A, as determined by XRD, correspond to the regions of negative electrostatic potential denoted on the MEP maps, Fig. 8. Forbidden pairs of nearest site occupancies were revealed by XRD, the required minimum distance for the M2–M2′ sites in channel B being estimated as 2.76–2.79 Å [4]. Much smaller forbidden distances were estimated for the channel A cations: 1.91–2.26 Å. The two symmetrical M1a sites, found by both ONIOM and PBC calculations after migration of Ca^{2+}, Na^+ and K^+ to the inner part of Channel A (Fig. 8), are nearly identical for all cations as they are separated by less than 0.4 Å. Though the cations at M1a site would be stabilized by an Al atom present at a T1 site, the M1a sites would host Na^+ cations also with Al at the highly favored T2 site, Table 2. The calculated internuclear distance which separates two Na^+ cations in channel A was estimated to be not smaller than 5.025 Å, and for the K^+ cations, not smaller than 4.305 Å. Larger values can be reached, depending on the Si, Al ordering. The locations of Na^+ and Ca^{2+} cations are in proximity to the ten-member ring of channel A and the cations

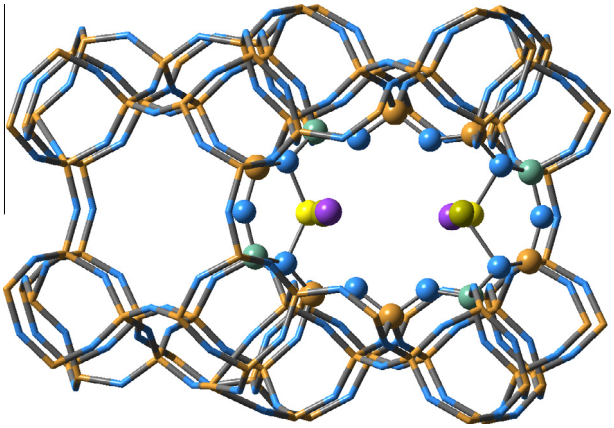

Fig. 8. The optimal positions of Ca^{2+}, Na^+ and K^+ cations after migration from the side rings into Channel A. K^+ cations are blue, Na^+ – yellow, Ca^{2+} – light green. Oxygen atoms are blue, Si – light brown, Al – green. (For interpretation of the references to color in this figure legend, the reader is referred to the web version of this article.)

are coordinated by oxygen atoms from the ring; the Na^+–O internuclear distances to the oxygen atoms are within 2.19–2.33 Å. The Ca^{2+} cations migration is strongly favored by Al → Si substitutions at T1 sites and the two cations are in this case separated by an internuclear distance of 4.850 Å. The K^+ cations are displaced away from the ten-member ring, as they keep strongly lengthened K^+–O internuclear distances of 2.65–2.70 Å. The K^+(M1a)-K^+(M1a′) distance varies within a narrow range, 4.305–4.380 Å, for the different Si, Al orderings. The calculated energies of different configurations do not account for the energy barriers for cations to cross the eight-member c-rings, but the free aperture of the c-rings of 2.8 Å [2] would allow Ca^{2+} and Na^+ cation permeability. The Ca^{2+} cations undergo minor displacement when shifting from site M1 to M1a; Na^+ cations can migrate from either the M2 sites, or M1 sites. K^+ and Ba^{2+} cations would not be able to diffuse free in channel C, but they reside preferably in Channel A. K^+ cations undergo a significant displacement upon migration from site M3 in the side eight-member rings to site M1a and this process requires significant energy.

The cation distribution at sites M1, M1a, M2 and M3 is different in the Al-rich heulandite and in the Si-rich clinoptilolite. Ca^{2+} are mostly occupying a site close to M3 in dehydrated heulandite [10], but their preferred sites in hydrated clinoptilolite were M1 and M2 [4]. According to our results, the small-size cations would be attracted more easily by the negative ESP in channel A, thus they would shift from the side rings towards the center of the channel and their exact position will be in proximity to a negative framework charge.

4. Conclusion

The properties of the zeolite clinoptilolite framework are correctly described by both the ONIOM method and by applying periodic boundary conditions (PBC) using density functional theory. The ordering by stability of different configurations with variable Si, Al and cation site occupancies are subject to minor discrepancies according to the two methods applied. Higher stabilization energies are determined by ONIOM for K^+ and Ca^{2+} cations. The cations can migrate towards the center of the large channel A, where the nucleophilic properties are stronger and this is evidenced by both ONIOM and PBC calculations; the energetics of such transitions is calculated. The much smaller c-parameter of the unit cell renders the long-range Si, Al substitution and cation site replications along the [001] direction unrealistic for a Si-rich zeolite such as clinoptilolite. The ONIOM method allows higher accuracy at much lower computational cost than PBC and though the effect of periodicity is lacking, this turns as advantage for studying Si, Al substitutions in the c-rings.

Acknowledgment

The computational results presented have been achieved using the Vienna Scientific Cluster (VSC).

Appendix A. Supplementary data

Supplementary data associated with this article can be found, in the online version, at http://dx.doi.org/10.1016/j.micromeso.2013.05.003.

References

[1] P. Misaelides, Micropor. Mesopor. Mater. 144 (2011) 15–18.
[2] Ch. Baerlocher, L.B. McCusker, D.H. Olson, Atlas of Zeolite Framework Types, sixth ed., Elsevier, Amsterdam, 2007.
[3] A. Alberti, Tschermaks Mineral. Petrogr. Mitt. 22 (1975) 25–37.
[4] K. Koyama, Y. Takéuchi, Z. Kristallogr. 145 (1977) 216–239.
[5] A. Sani, G. Vezzalini, P. Ciambelli, M.T. Rapacciuolo, Micropor. Mesopor. Mater. 31 (1999) 263–270.
[6] T. Armbruster, Am. Mineral. 78 (1993) 260–264.
[7] T. Armbruster, M.E. Gunter, Am. Mineral. 76 (1991) 1872–1883.
[8] K. Sugiyama, Y. Takéuchi, Stud. Surf. Sci. Catal. 28 (1986) 449–456.
[9] E. Galli, G. Gottardi, H. Mayer, A. Preisinger, E. Passaglia, Acta Cryst. B 39 (1983) 189.
[10] W.J. Mortier, J.R. Pearce, Am. Mineral. 66 (1981) 309–314.
[11] A.O. Larsen, F.S. Nordrum, N. Döbelin, Th. Armbruster, O.V. Petersen, M. Erambert, Eur. J. Mineral. 17 (2005) 143–153.
[12] M. Sacerdoti, G. Lucchetti, Micropor. Mesopor. Mater. 131 (2010) 310–313.
[13] M. Johnson, D. O'Connor, P. Barnes, C.R.A. Catlow, S.L. Owens, G. Sankar, R. Bell, S.J. Teat, R. Stephenson, J. Phys. Chem. B 107 (2003) 942–951.
[14] D. Barthomeuf, Catal. Rev. Sci. Eng. 38 (1996) 521.
[15] E.A. Pidko, P. Mignon, P. Geerlings, R.A. Schoonheydt, R.A. van Santen, J. Phys. Chem. C 112 (2008) 5510–5519.
[16] P. Mignon, E.A. Pidko, R.A. Van Santen, P. Geerlings, R.A. Schoonheydt, Chem. Eur. J. 14 (2008) 5168–5177.
[17] Y.M. Channon, C.R.A. Catlow, R.A. Jackson, S.L. Owens, Micropor. Mesopor. Mater. 24 (1998) 153–161.
[18] A.R. Ruiz-Salvador, A. Gomez, D. Day-Lewis, C.R.A. Catlow, L.M. Rodriguez-Albelo, L. Montero, G. Rodriguez-Fuentes, Phys. Chem. Chem. Phys. 2 (2000) 1803–1813.
[19] J.B. Nicholas, Top. Catal. 4 (1997) 157–171.
[20] J.C. White, J.B. Nicholas, A.C. Hess, J. Phys. Chem. B 101 (1997) 590–595.
[21] S. Grigoras, T.H. Lane, J. Comput. Chem. 8 (1987) 84–93.
[22] J.-R. Hill, C. Freeman, B. Delley, J. Phys. Chem. A 103 (1999) 3772–3777.
[23] T. Yumura, M. Takeuchi, H. Kobayashi, Y. Kuroda, Inorg. Chem. 48 (2009) 508–517.
[24] E.L. Uzunova, H. Mikosch, J. Phys. Chem. B 108 (2004) 6981–6987.
[25] H. Mikosch, E.L. Uzunova, G. St. Nikolov, J. Phys. Chem. B 109 (2005) 11119–11125.
[26] F. Corà, C.R.A. Catlow, J. Phys. Chem. B 105 (2001) 10278–10281.
[27] S. Dapprich, I. Komáromi, K.S. Byun, K. Morokuma, M.J. Frisch, J. Mol. Struct. (Theochem.) 462 (1999) 1–21.
[28] J.T. Fermann, T. Moniz, O. Kiowski, T.J. McIntire, S.M. Auerbach, T. Vreven, M.J. Frisch, J. Chem. Theory Comput. 1 (2005) 1232–1239.
[29] T. Vreven, M.J. Frisch, K.N. Kudin, H.B. Schlegel, K. Morokuma, Mol. Phys. 104 (2006) 701–714.
[30] Gaussian 09, Revision C.01, M. J. Frisch, G. W. Trucks, H. B. Schlegel, et al., Gaussian Inc., Wallingford, CT, 2009.
[31] J.P. Perdew, K. Burke, M. Ernzerhof, Phys. Rev. Lett. 77 (1996) 3865–3868.
[32] J.P. Perdew, K. Burke, M. Ernzerhof, Phys. Rev. Lett. 78 (1997) 1396.
[33] W.J. Pietro, M.M. Francl, W.J. Hehre, D.J. Defrees, J.A. Pople, J.S. Binkley, J. Am. Chem. Soc. 104 (1982) 5039–5048.
[34] K.D. Dobbs, W.J. Hehre, J. Comput. Chem. 7 (1986) 359–378.
[35] M.M. Francl, W.J. Pietro, W.J. Hehre, J.S. Binkley, D.J. DeFrees, J.A. Pople, M.S. Gordon, J. Chem. Phys. 77 (1982) 3654–3665.
[36] V.A. Rassolov, J.A. Pople, M.A. Ratner, T.L. Windus, J. Chem. Phys. 109 (1998) 1223–1229.
[37] V.A. Rassolov, M.A. Ratner, J.A. Pople, P.C. Redfern, L.A. Curtiss, J. Comput. Chem. 22 (2001) 976–984.
[38] A.E. Reed, L.A. Curtiss, F. Weinhold, Chem. Rev. 88 (1988) 899–926.
[39] F. Weinhold, J.E. Carpenter, The Structure of Small Molecules and Ions, Plenum, 1988.
[40] T. Vreven, K.S. Byun, I. Komáromi, S. Dapprich, J.A. Montgomery Jr., K. Morokuma, M.J. Frisch, J. Chem. Theory Comput. 2 (2006) 815–826.
[41] F. Clemente, T. Vreven, M.J. Frisch, in: C. Matta (Ed.), Quantum Biochemistry, vol. 1, Wiley-VCH, Weinheim, 2010, pp. 61–83.
[42] F. Weigend, R. Ahlrichs, Phys. Chem. Chem. Phys. 7 (2005) 3297–3305.
[43] M. Kaupp, P.V. Schleyer, H. Stoll, H. Preuss, J. Chem. Phys. 94 (1991) 1360–1366.
[44] C. Lee, W. Yang, R.G. Parr, Phys. Rev. B 37 (1988) 785–789.
[45] B. Miehlich, A. Savin, H. Stoll, H. Preuss, Chem. Phys. Lett. 157 (1989) 200–206.
[46] A.D. Becke, J. Chem. Phys. 98 (1993) 5648–5652.
[47] A.K. Rappé, C.J. Casewit, K.S. Colwell, I.I.I. Goddard, J. Am. Chem. Soc. 114 (1992) 10024–10035.
[48] N. Bresciani-Pahor, M. Calligaris, G. Nardin, L. Randaccio, E. Russo, J. Chem. Soc., Dalton Trans. (1980) 1511–1514.
[49] T.W. Hambley, J.C. Taylor, J. Solid State Chem. 54 (1984) 1–9.
[50] R.D. Shannon, Acta Cryst. A 32 (1976) 751–767.
[51] G. Klopman, Chemical Reactivity and Reaction Paths, J. Wiley, New York, 1974.
[52] A. Hinchliffe, Computational Quantum Chemistry, J. Wiley, Chichester, New York, 1988.
[53] P. Vassileva, D. Voikova, J. Hazard. Mater. 170 (2009) 948–953.
[54] J.L. Palmer, M.E. Gunter, Am. Mineral. 86 (2001) 431–437.
[55] W. Wooyong Um, Ch. Papelis, Am. Mineral. 88 (2003) 2028–2039.
[56] S. Ogihara, A. Iijima, Eur. J. Mineral. 2 (1990) 819–826.